Turkish Journal of Electrical Engineering & Computer Sciences

http://journals.tubitak.gov.tr/elektrik/

Research Article

Turk J Elec Eng & Comp Sci
(2016) 24: 3105 – 3122

doi:10.3906/elk-1406-35

Power system harmonic reduction and voltage control using DFIG converters as an active filter

Seyyed Mostafa NOSRATABADI, Eskandar GHOLIPOUR*
Department of Electrical Engineering, Faculty of Engineering, University of Isfahan, Isfahan, Iran

Received: 07.06.2014 • **Accepted/Published Online:** 05.03.2015 • **Final Version:** 15.04.2016

Abstract: In this paper, for bus voltage control and to reduce power system harmonics, the active filtering technique is used in the mechanism of wind turbine control. Here a grid-connected doubly fed induction generator (DFIG) is considered in a wind turbine. In addition to harmonics that are related to the DFIG, a nonlinear load is also added to the system to simulate loads that produce more harmonics. The active filtering approach is implemented to mitigate current and voltage harmonics, which is one of the main concerns of distribution systems. A bus voltage control strategy is also used for this purpose. The main advantages of this article are (i) using a simple and effective active filtering technique and (ii) applying a voltage control method to mitigate the mentioned harmonics. The presented methodology is examined in both local and remote control conditions and also for both normal and contingency (load change) situations. Simulation results obtained from applying the presented method on a distribution test system confirm suitable performance of the proposed strategy to mitigate current and voltage harmonics.

Key words: Doubly fed induction generator (DFIG), harmonic reduction, active filter, voltage control, nonlinear load

1. Introduction

Nowadays, renewable energy resources are increasingly used in power systems. Wind energy is one of them, whose use has increased in the last decade. This growth is partly because of the technological improvement of wind turbines, which has led to decreased wind power costs, allowing this energy source to compete against another conventional generation methods. Many wind farms utilize doubly fed induction generators (DFIGs) in their structures. DFIGs possess several advantages, including speed control and reducing flicker and four-quadrant active and reactive power control capabilities [1,2].

Since the most optimal turbine rotor speed can be utilized at any given wind speed, wind turbines based on the DFIG give a higher mechanical output power. From an economic point of view, the DFIG is more beneficial due to the rate of power converters. This power is around 30% of nominal power and so their power converters are cheaper [1]. DFIGs are widely used together with voltage source converters (VSCs) in wind turbine applications [2,3]. These power electronic interfaces are connected between the rotor of the generator and the grid. They can provide some ancillary services, such as harmonic mitigation, in addition to real power control [4]. Although wind farms generate harmonics, the converters can be controlled such that this control mitigates the harmonics of the system. The effect of DFIGs on power system harmonics has been investigated [5–8]. In recent years, a power quality problem (especially harmonic reduction related to power systems) with DFIGs has been demonstrated by several workers [9–19] who have considered this serious problem.

*Correspondence: e.gholipour@eng.ui.ac.ir

A control method for a wind energy conversion system meant to partially operate as an active filter is described in [9]. The control is defined in an equivalent reference frame obtained by applying Park transformation to the three-phase quantities. The control system includes the zero-sequence component that enables the compensation of zero-sequence harmonics. A control strategy to achieve simultaneously active and reactive power generation with the addition of active filter capability to a variable speed DFIG wind energy system is also presented in [10]. It shows that power loss reduction and mitigation of current and voltage harmonics can be obtained using the active filter capability for a variable speed DFIG wind energy system. A new modulation technique used in a shunt active filter to improve the output current harmonics of a wind energy conversion system, including a permanent magnet synchronous generator (PMSG) and an AC-to-DC converter is proposed in [11]. The design and analysis of a control scheme for a DFIG based wind energy generation under unbalanced grid voltage conditions are presented in [12]. The control objectives are: (i) to limit the rotor currents, (ii) to suppress ripples in the torque, and (iii) to suppress the dc-link voltage fluctuation through converter controls. A hybrid current control scheme is introduced in [13]. This method is implemented in the rotor-side and grid-side converters of the DFIG to enhance the voltage ride-through capacities of DFIG-based wind turbines. In [14] analysis of power quality is presented on the effects of high penetration electric vehicles and renewable energy based generator systems, including wind turbines, grid connected photovoltaic, and fuel cell power generation units. Application of a five-leg converter in a DFIG for wind energy conversion systems is investigated in [15]. The five-leg structure and its PWM control are studied and performances are compared with the classical six-leg topology. The main drawback of the five-leg converter with respect to the six-leg back-to-back converter is the need to increase the dc-link voltage for the same operation point. Reference [16] describes a solution to protect sensitive loads against voltage disturbances that is based on a series power line conditioner. The goal of the proposed design is that the load does not suffer from considerable input voltage variations. To achieve that, a proportional-resonant controller and a reference generator block based on a low-gain PLL are used, which avoids a sag detection block.

A proportional resonance control strategy in the stationary reference frame to minimize rotor current harmonics and torque pulsations is developed in [17]. A vector control scheme for a stand-alone generator based on a wound rotor induction machine with rotor side control is described in [18]. The primary objective of the control scheme is to maintain constant voltage and frequency at the output of the generator. An approach for simultaneous power generation and harmonic current mitigation using a variable speed wind energy conversion system with a DFIG is presented in [19]. A control strategy is proposed to upgrade the DFIG control to achieve simultaneously a green active and reactive power source. The mitigation of the voltage harmonics is an important task that cannot be performed by current source inverters (CSIs).

In this paper, the active filtering approach is used to mitigate harmonics current of the power system. For this purpose, the controller in the wind turbine system is used as an active filter. In this system, grid side converter (GSC) control is used to generate the currents in such a way that they contain harmonics equal and 180 degree out of phase with harmonics of nonlinear load currents causing cancellation of nonlinear load current harmonics. In addition, a bus voltage control strategy is used for this harmonic reduction in GSC too. In this strategy, the voltage of the DFIG installation bus, which is measured, is applied to the GSC control to perform the proposed voltage control strategy. These are employed at the same time in the power system and can manage the harmonic reduction in both normal and contingency (load change) conditions.

The paper is organized as follows. The structure of the grid connected DFIG wind turbine is studied in section 2. Section 3 describes vector control of the DFIG, including its grid side and rotor side control. The

structure of the active filtering approach and its usage in the control mechanism are studied in section 4. The under study system is introduced in section 5. Simulation results in MATLAB/SIMULINK are presented in section 6. Finally, some concluding remarks are reviewed.

2. Grid connected DFIG

Figure 1 shows the block diagram of the grid connected DFIG wind turbine. In this figure, the stator of the DFIG is directly connected to the grid. A back-to-back PWM converter is connected between the rotor and the grid. It is used to control the DFIG. The back-to-back converter consists of a rotor side converter and a grid side converter connected by a DC link bus. The purpose of the grid side converter is to provide constant DC link voltage, and the rotor side converter controls the active and reactive power supplied to the power system network [2]. By using two back-to-back converters bidirectional power flow capability is achieved [2,20]. The voltage and flux equations of the DFIG are as follows [21]:

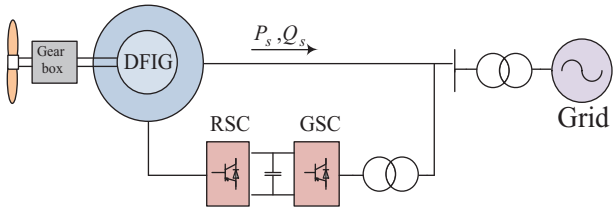

Figure 1. Block diagram of grid connected DFIG wind turbine.

$$\begin{aligned}
V_{ds} &= R_s i_{ds} + \tfrac{d}{dt}\psi_{ds} - \omega_s \psi_{qs} \\
V_{qs} &= R_s i_{qs} + \tfrac{d}{dt}\psi_{qs} + \omega_s \psi_{ds} \\
V_{dr} &= R_r i_{dr} + \tfrac{d}{dt}\psi_{dr} - \omega_r \psi_{qr} \\
V_{qr} &= R_r i_{qr} + \tfrac{d}{dt}\psi_{qr} + \omega_r \psi_{dr} \\
\psi_{dr} &= L_r i_{dr} + L_m i_{ds} \\
\psi_{qr} &= L_r i_{qr} + L_m i_{qs} \\
\psi_{ds} &= L_s i_{ds} + L_m i_{dr} \\
\psi_{qs} &= L_s i_{qs} + L_m i_{qr}
\end{aligned} \tag{1}$$

The electromagnetic torque is expressed as follows:

$$T_{em} = \frac{3}{2}(\psi_{ds} i_{qs} - \psi_{qs} i_{ds}) \tag{2}$$

The active and reactive powers of the DFIG can be determined using the following equations:

$$P_s = \frac{3}{2}(V_{ds} i_{ds} + V_{qs} i_{qs}) \tag{3}$$

$$Q_s = \frac{3}{2}(V_{ds} i_{qs} - V_{qs} i_{ds}), \tag{4}$$

where V, R, i, $L-$, ψ, and ω are voltage, resistance, current, inductance, flux, and angular speed of the DFIG, respectively. P and Q are active and reactive power. The $d-q$ subscripts demonstrate $d-q$ components and r, s, and m subscripts demonstrate rotor, stator, and magnetizing values, respectively.

3. Vector control of the DFIG

3.1. Grid side converter control

The grid side converter is used to keep the DC link voltage constant. The d axis current is used to regulate the DC link voltage and the q axis current component is used to regulate the reactive power [2]. The grid side vector control scheme is presented in Figure 2. The upper part of the diagram is used to determine $d-axis$ parameters and the lower part of diagram is used to determine $q-axis$ parameters. The difference between the reference DC voltage and the measured DC voltage is the input of the DC link PI controller. i_{dref} is the output of the DC link PI controller. The error $(i_{dref}--i_{dmeas})$ is the input of the current PI controller. The output of this controller is the auxiliary reference voltage $V\prime_d$. The actual reference voltage is shown in (5) [22]:

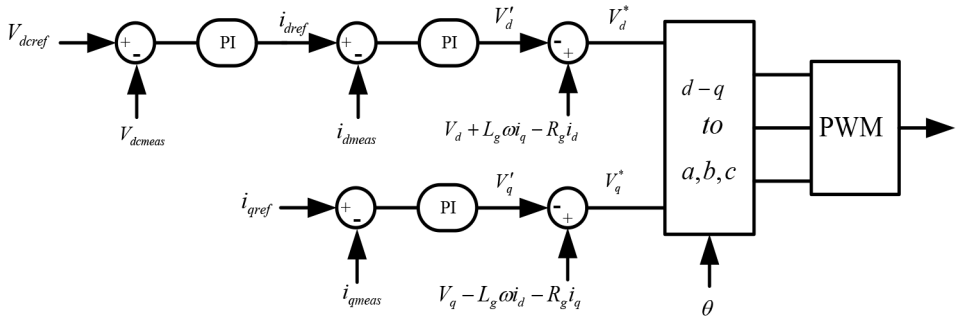

Figure 2. Grid side converter control system.

$$V_d^* = V_d + L_g\omega.i_q - R_g i_d - V_d' \tag{5}$$

The g subscript demonstrates grid side value. The $q-axis$ is aligned along the stator voltage vector and so i_{qref} is set to be zero. Moreover, it is proposed to control the bus voltage; at first with setting an error obtained from subtracting the measured voltage and reference voltage and control of that with a PI controller, i_{qref} can be calculated. Then the difference between i_{qref} and i_{qmeas} is the input for the current PI controller and the output of this PI controller is auxiliary voltage $V\prime_q$. Finally (6) can be used to determine actual voltage [22].

$$V_q^* = V_q - L_g\omega i_d - R_g i_q - V_q' \tag{6}$$

3.2. Rotor side converter control

The rotor side converter is designated to control the DFIG output power to the grid. It is used to regulate the power factor at the DFIG terminals [23]. The stator active and reactive powers are the inputs of rotor side converter control. The block diagram of the rotor side converter control is shown in Figure 3; the upper part describes the $d-axis$ variables and the lower part deals with the $q-axis$ variables. The following equations represent the $d-axis$ reference current [24]:

$$T_e = \frac{P_m - P_{loss}}{\omega_r} \tag{7}$$

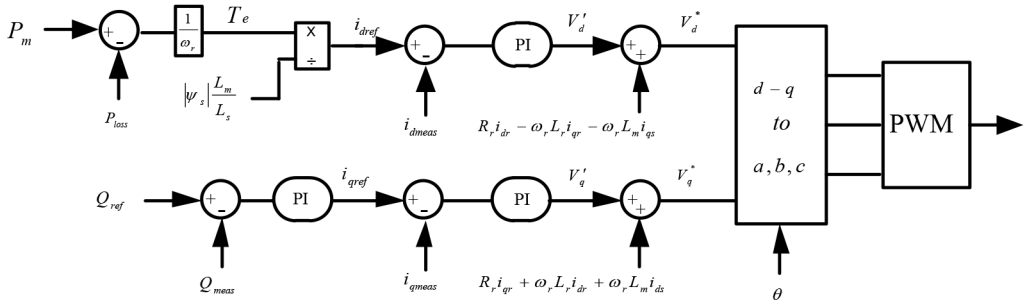

Figure 3. Rotor side converter control system.

where P_m, P_{loss}, and ω_r are mechanical power, loss power, and rotor speed, respectively. Then the mentioned current is calculated as

$$i_{dref} = \frac{T_e}{|\psi_s| .L_m/L_s} \tag{8}$$

The difference between i_{dref} and i_{dmeas} is the input of the current controller. The output of this controller is $V\prime_d$. The V_d^* can be determined by the following equation [22]:

$$V_d^* = V_d' + R_r i_{dr} - \omega_r L_r i_{qr} - \omega_r L_m i_{qs} \tag{9}$$

The q – *axis* reference current is obtained from the instantaneous reactive power. The reactive power error $(Q_{ref} - -Q_{meas})$ is the input of reactive power controller and the output of this PI controller determines i_{qref}. The difference between i_{qref} and i_{qmeas} is the input of the current PI controller. The output of the current controller is auxiliary voltage $V\prime_q$. Finally the q axis actual reference voltage is as follows [22]:

$$V_q^* = V_q' + R_r i_{qr} + \omega_r L_r i_{dr} + \omega_r L_m i_{ds} \tag{10}$$

4. Active filtering technique

Harmonic currents are injected into the power system by the nonlinear loads (NLLs). That causes an increase in the current harmonic distortion of the PCC and other buses of the power system. Current harmonic distortion, in turn, causes voltage distortion. Figure 4 shows a NLL connected to the power system via DFIG bus. This load injects harmonic current into the grid. The wind turbine system can be used as an active filter to sink the harmonics injected by the NLL. In this paper, the grid side converter is used to generate the NLL currents (i_{La}, i_{Lb}, i_{Lc}) in such a way that they contain harmonics equal and 180 degree out of phase with harmonics of NLL currents. It cancels NLL current harmonics [9]. This is why the nonlinear load currents should be measured firstly. Then the *abc* to $\alpha - \beta$ (stationary reference frame) transformation is used to transform the measured load currents (i_a, i_b, i_c) into $\alpha - \beta$ reference frame. The NLL current is the sum of the fundamental frequency and other harmonics as follows:

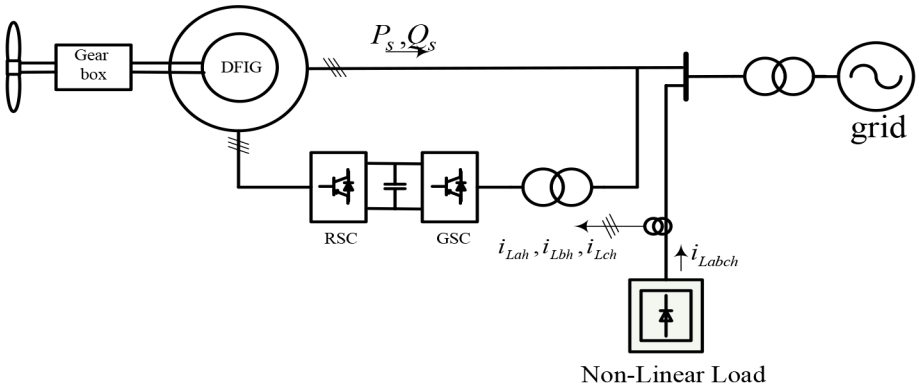

Figure 4. Wind energy conversion system associated with nonlinear load.

$$i_{L\alpha} = i_{L\alpha f} + i_{L\alpha h} \tag{11}$$

$$i_{L\beta} = i_{L\beta f} + i_{L\beta h}, \tag{12}$$

where $(i_{L\alpha h},\ i_{L\beta h})$ and $(i_{L\alpha f},\ i_{L\beta f})$ are harmonic and fundamental components of NLL current.

Based on (11) and (12), harmonic components of load current can be expressed by subtracting load and its fundamental current components. In order to separate the harmonic of NLL, the scheme represented in Figure 5 can be used. In this figure, the park transformation is used to express the $\alpha-\beta$ current components to $d-q$ (synchronous) reference frame. The fundamental component can be extracted from $\alpha-\beta$ components by a high selectivity filter. The high selectivity filter is a band pass filter as follows [19]:

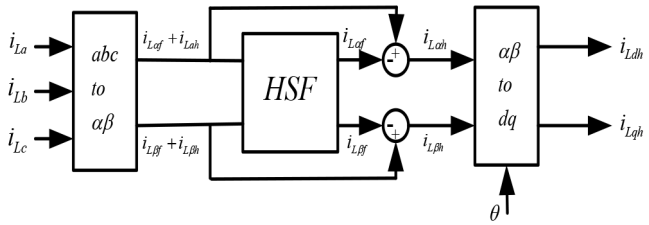

Figure 5. Harmonic detachment of load current.

$$H(s) = \frac{\hat{i}_{\alpha\beta}}{i_{\alpha\beta}} = K\frac{(s+K)+j\omega}{(s+K)^2+\omega^2} \tag{13}$$

In this equation, $i_{\alpha\beta}$ and $i_{\alpha\beta}$ represent inputs and outputs of the filter, respectively. They consist of two components as follows:

$$i_{\alpha\beta}(s) = i_{\alpha}(s) + ji_{\beta}(s) \tag{14}$$

$$\hat{i}_{\alpha\beta}(s) = \hat{i}_{\alpha}(s) + j\hat{i}_{\beta}(s) \tag{15}$$

Using (13)–(15) the following equations are found:

$$\hat{i}_{\alpha}(s) = \frac{K}{S}\left[i_{\alpha}(s) - \hat{i}_{\alpha}(s)\right] - \frac{\omega}{s}\hat{i}_{\beta}(s) \tag{16}$$

$$\hat{i}_{\beta}(s) = \frac{K}{S}\left[i_{\beta}(s) - \hat{i}_{\beta}(s)\right] + \frac{\omega}{s}\hat{i}_{\alpha}(s), \tag{17}$$

where $\hat{i}_{\alpha}$ and $\hat{i}_{\beta}$ are fundamental components of the high selectivity filtered load currents, ω is the nominal frequency, and K is a constant value. Figure 6 illustrates the structure of high selectivity filter represented by (16) and (17).

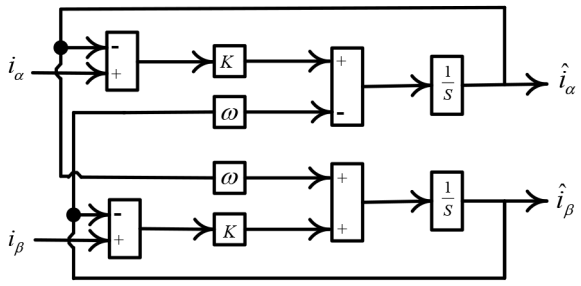

Figure 6. High selectivity filter.

Furthermore, the under study grid side converter control scheme is shown in Figure 7. In this scheme a new voltage control method is proposed; using this method, the voltage of the DFIG bus can be controlled. As can be seen in Figure 7, after measuring the voltage of the DFIG bus and comparing with the reference value, a PI controller is applied to it and its output will be i_{qref}, which we need for the input of the GSC control system as illustrated in Figure 2. In this control strategy, the voltage $V_{Bus-meas}$ is the voltage of the DFIG installation bus, which is measured and applied to perform the proposed voltage control strategy.

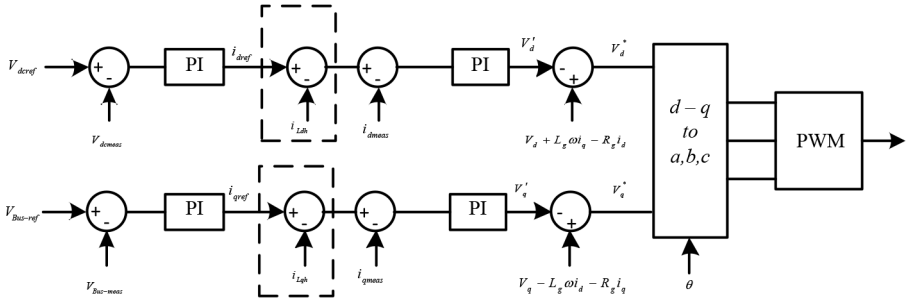

Figure 7. Under study grid side converter control.

To clarify the main details related to the proposed methodology, the following statements can be briefly made. In this methodology, using active filtering based on GSC control to keep the DC link voltage constant in a grid connected DFIG controller and also using a voltage control strategy to generate the input current for the GSC, harmonic reduction can be performed. This issue can be managed in both normal and contingency conditions too. To show the effectiveness of the proposed method, simulation aspects are performed on a test system.

5. Under study system

Figure 8 represents a modified single line diagram of the under study system [25]. The system consists of a 13.8 KV three-feeder distribution subsystem connected to a large network. The main grid is represented by a three

phase 69 KV voltage source with 1000 MVA short circuit capacity and X/R ratio of 22.2. The distribution feeders are connected to the main grid through a 69 KV/13.8 KV, 15 MVA transformer. The point of common coupling (PCC) is fed through a 1.5 MVAR fixed shunt capacitor bank. L1 to L5 are local linear loads and L6 is a nonlinear load. The DG is a 5 MVA DFIG wind turbine connected to the network through a transformer. The studied system parameters are presented in the Appendix.

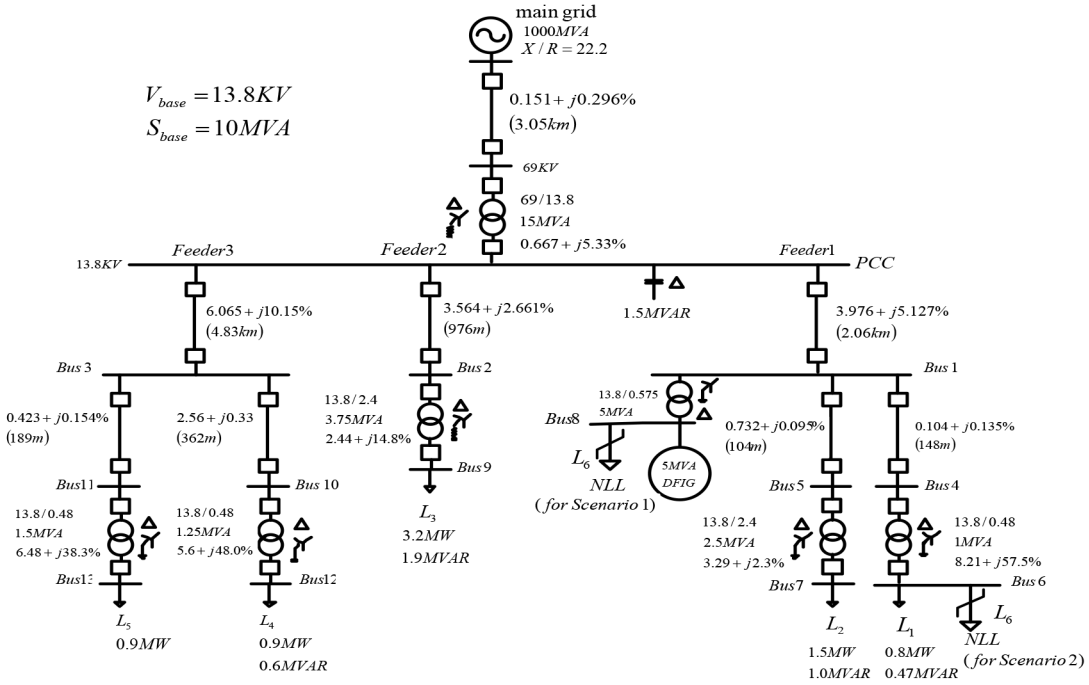

Figure 8. Single line diagram of the under study system.

6. Simulation results

In this study, in order to investigate the performance of active filtering technique on reduction of harmonics of the power system, MATLAB-SIMULINK and Simpower Toolbox are used. In order to evaluate the performance of the under study active filtering technique, harmonics level and THD indices are used. The NLL is simulated by means of a diode rectifier feeding a RL load. Figure 9 and Table 1 show the NLL harmonic spectrum and characteristics, respectively. It is noteworthy that the bus voltage control strategy is applied to the DFIG installation bus, which means $V_{Bus-meas}$ (presented in the previous section) is measured at bus 8.

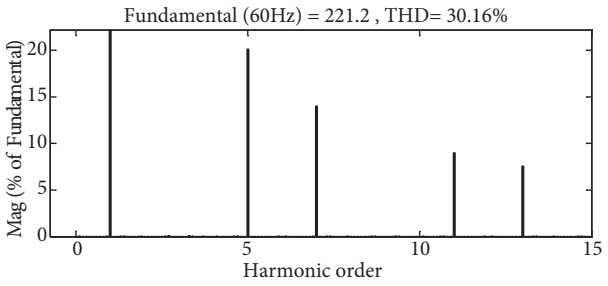

Figure 9. Harmonic spectrum of the used NLL.

Table 1. NLL harmonic characteristics.

Harmonic order	1st (60 Hz) (Fundamental)	5th	7th	11th	13th	THD
Magnitude (%)	100	20	14.02	9	7.57	30.16

To verify the effectiveness of the proposed method the NLL is considered in four scenarios. The first one is local control in which the NLL is connected to bus 8 (DFIG bus). The second one is remote control in which the NLL is connected to bus 6 and the proposed method is applied to mitigate the harmonics of the NLL. To have a suitable verification for the proposed method for the NLL change as a contingency condition, two other scenarios are considered too. In scenario no. 3, the step change at the NLL is considered for local condition of the load and in scenario no. 4, this change is considered for remote control condition.

6.1. Scenario no. 1: local control

As mentioned, in this scenario, the NLL is placed at bus 8 to investigate the performance of the proposed method for harmonic reduction in a local condition. The results related to DFIG and PCC bus voltage signals (with and without active filtering approach and bus voltage control method) are summarized in Tables 2 and 3 for this scenario. The study is undertaken for three types of nonlinear loads: 100 A, 2000 A, and 4000 A. As shown in Table 2, by the use of under study active filtering and bus voltage control techniques in the DFIG control, the THD of voltage values for load types 100 A, 2000 A, and 4000 A are 0.33%, 3.63%, and 6.58%, respectively. The THD of voltage values for these loads without using the active filtering and bus voltage control techniques in the DFIG control are 0.86%, 9.85%, and 14.46%, respectively, too.

Table 2. Comparison of THD of DFIG bus voltages for scenario no. 1.

	THD ($V_{DFIGBus}$) (%)			
	With bus voltage control		Without bus voltage control	
Load type	Without active filtering	With active filtering	Without active filtering	With active filtering
100 A	0.78	**0.33**	0.86	0.67
2000 A	9.73	**3.63**	9.85	3.95
4000 A	14.22	**6.58**	14.46	6.82

According to the results, it can be concluded that the proposed method decreases THD of voltages. The results related to PCC bus voltages are shown in Table 3. As can be seen, the THD values for the mentioned loads are decreased so that using the proposed method for 100 A, 2000 A, and 4000 A, the THD values are 0.33%, 3.61%, and 6.54%, but without using this method these values are increased to 0.86%, 9.81%, and 14.39%, respectively, which shows the effectiveness of the proposed technique. Tables 4 and 5 show THD values for DFIG and PCC buses current signals. As shown in Table 4, by the use of under study active filtering and bus voltage control techniques in DFIG control, the THD of DFIG bus current values for load types 100 A, 2000 A, and 4000 A are 0.32%, 4.07%, and 6.89%, respectively. The THD of current values for these loads without using the active filtering and bus voltage control techniques in the DFIG control are 0.79%, 8.55%, and 16.14%, respectively. Furthermore, it can be seen in Table 5 for PCC bus current that the proposed method effectively decreases the THD percent related to current signals.

Table 3. Comparison of THD of PCC bus voltages for scenario no. 1.

	THD (V $_{PCCBus}$) (%)			
	With bus voltage control		Without bus voltage control	
Load type	Without active filtering	With active filtering	Without active filtering	With active filtering
100 A	0.78	**0.33**	0.86	0.66
2000 A	9.73	**3.61**	9.81	3.90
4000 A	14.20	**6.54**	14.39	6.81

Table 4. Comparison of THD of DFIG bus currents for scenario no. 1.

	THD (I $_{DFIGBus}$) (%)			
	With bus voltage control		Without bus voltage control	
Load type	Without active filtering	With active filtering	Without active filtering	With active filtering
100 A	0.64	**0.32**	0.79	0.53
2000 A	8.34	**4.07**	8.55	4.30
4000 A	15.81	**6.89**	16.14	7.23

Table 5. Comparison of THD of PCC bus currents for scenario no. 1.

	THD (I $_{PCCBus}$) (%)			
	With bus voltage control		Without bus voltage control	
Load type	Without active filtering	With active filtering	Without active filtering	With active filtering
100 A	0.77	**0.37**	0.92	0.51
2000 A	9.98	**4.99**	10.17	5.25
4000 A	16.79	**8.49**	16.84	8.79

For instance, Figures 10 and 11 show the PCC bus current and voltage curves, respectively, and Figures 12 and 13 show the DFIG bus current and voltage curves, respectively. Each of them is with and without active filtering and bus voltage control for load type 4000 A. They illustrate the effectiveness of the proposed method based on the numerical results in Tables 2 to 5. To show the current harmonic spectrums for the mentioned tables, Figures 14 and 15 can be used to compare the conditions of with and without proposed method.

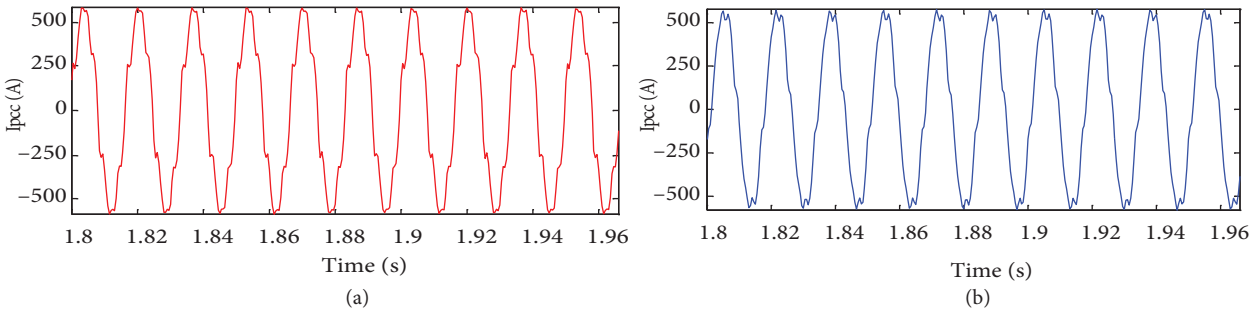

Figure 10. PCC bus current for load type 4000 A in scenario no. 1; (a) without control, (b) with proposed control method.

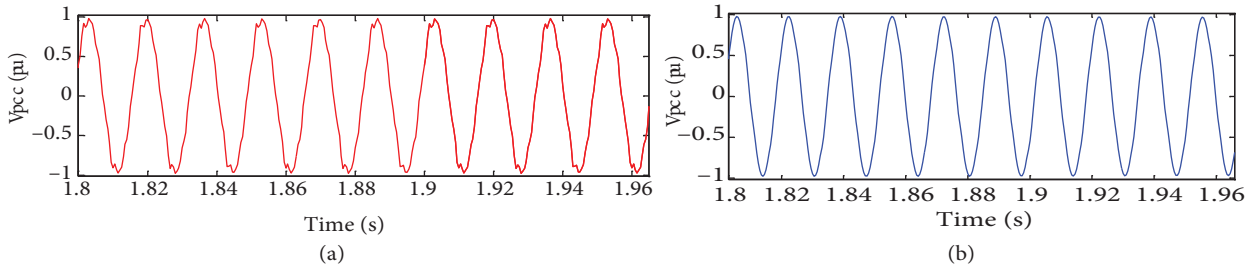

Figure 11. PCC bus voltage for load type 4000 A in scenario no. 1; (a) without control, (b) with proposed control method.

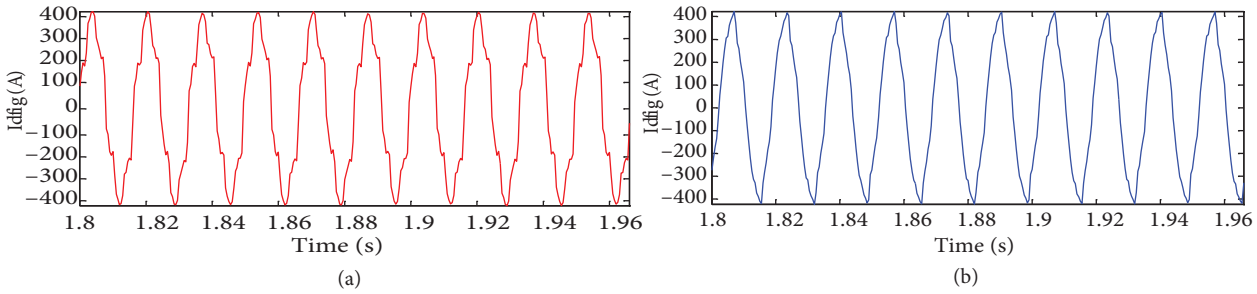

Figure 12. DFIG bus current for load type 4000 A in scenario no. 1; (a) without control, (b) with proposed control method.

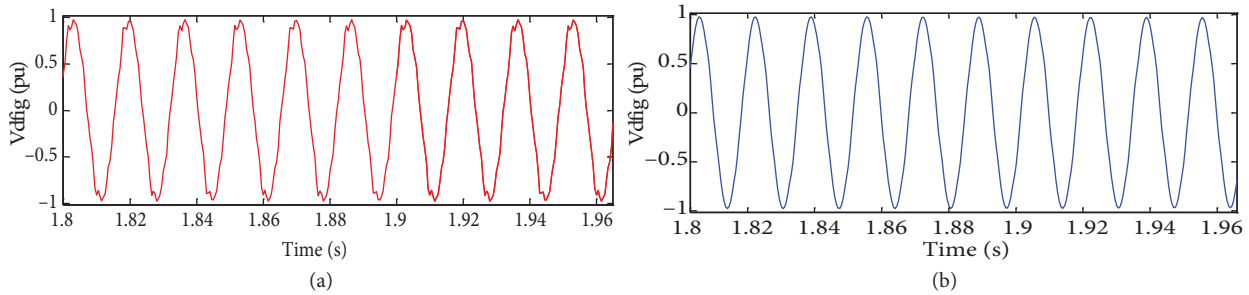

Figure 13. DFIG bus voltage for load type 4000 A in scenario no. 1 (a) without control, (b) with proposed control method.

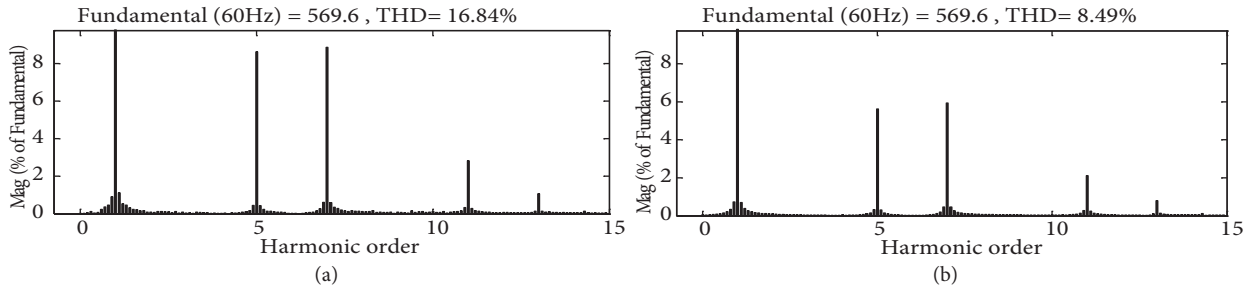

Figure 14. PCC bus current harmonic spectrum for load type 4000 A in scenario no. 1; (a) without control, (b) with proposed control method.

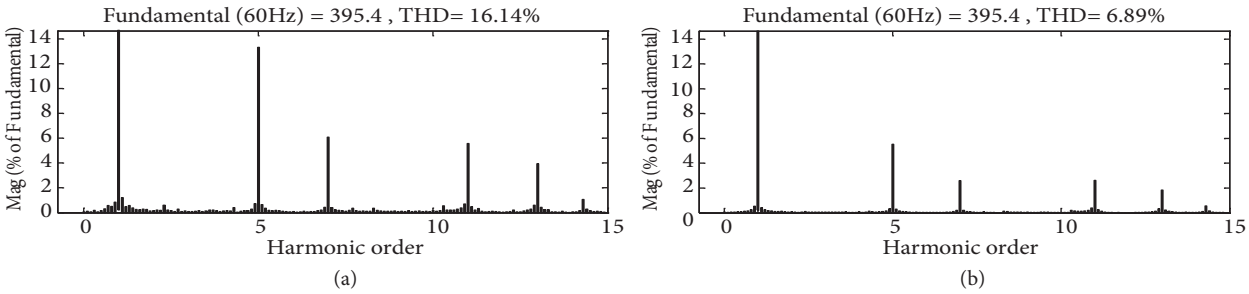

Figure 15. DFIG bus current harmonic spectrum for load type 4000 A in scenario no. 1; (a) without control, (b) with proposed control method.

6.2. Scenario no. 2: remote control

In this scenario, the NLL is placed at bus 6 to investigate the performance of the proposed method for harmonic reduction in a remote condition. The results of DFIG and PCC bus voltage signals (with and without active filtering approach and bus voltage control method) are summarized in Tables 6 and 7 for this scenario. Here the study is done for three types of NLLs: 100 A, 2000 A, and 4000 A. As shown in Table 6, using under study active filtering and bus voltage control techniques in the DFIG control, the THD of voltage values for load types 100 A, 2000 A, and 4000 A are 0.23%, 1.50%, and 1.70%, respectively. The THD of voltage values for these loads without using the active filtering and bus voltage control techniques in the DFIG control are 0.58%, 3.18%, and 3.63%, respectively.

Table 6. Comparison of THD of DFIG bus voltages for scenario no. 2.

	THD ($V_{DFIGbus}$) (%)			
	With bus voltage control		Without bus voltage control	
Load type	Without active filtering	With active filtering	Without active filtering	With active filtering
100 A	0.55	**0.23**	0.58	0.47
2000 A	2.89	**1.50**	3.18	1.96
4000 A	3.37	**1.70**	3.63	2.20

Therefore, it can be concluded that the proposed method decreases THD of voltages. The results related to PCC bus voltages are shown in Table 7. As can be seen, the THD values for the mentioned loads are decreased so that using proposed method for 100 A, 2000 A, and 4000 A the THD values are 0.23%, 1.48%, and 1.68%, but without using this method these values are increased to 0.58%, 3.14%, and 3.62%, respectively, which shows the effectiveness of the proposed technique. Tables 8 and 9 show THD values for DFIG and PCC buses current signals. As shown in Table 8, by the use of the proposed control techniques in the DFIG control, the THD of current values for load types 100 A, 2000 A, and 4000 A are 0.50%, 2.14%, and 1.97%, respectively. The THD of current values for these loads without using control techniques are 1.48%, 4.93%, and 5.24%, respectively. It can be seen in Table 9 for PCC bus current without and with the proposed method effectively THD values related to current signals decrease from 1.36, 5.32, and 5.18 to 0.42, 2.53, and 2.34 for the mentioned load types, respectively. In this scenario, Figures 16 and 17 show the PCC bus current and voltage curves, respectively, and Figures 18 and 19 show the DFIG bus current and voltage curves, respectively. Each of them is with and without the proposed control method for load type 4000 A. They illustrate the effectiveness of the proposed method based on the numerical results for remote control condition and harmonic reduction application, which

are clarified in Tables 6 to 9. Here, to show the current harmonic spectrums for the mentioned tables, Figures 20 and 21 can be used to compare the conditions with and without the proposed method too.

Table 7. Comparison of THD of PCC bus voltages for scenario no. 2.

	THD (V_{PCCbus}) (%)			
	With bus voltage control		Without bus voltage control	
Load type	Without active filtering	With active filtering	Without active filtering	With active filtering
100 A	0.41	**0.23**	0.58	0.47
2000 A	2.97	**1.48**	3.14	1.85
4000 A	3.43	**1.68**	3.62	2.15

Table 8. Comparison of THD of DFIG bus currents for scenario no. 2.

	THD ($I_{DFIGbus}$) (%)			
	With bus voltage control		Without bus voltage control	
Load type	Without active filtering	With active filtering	Without active filtering	With active filtering
100 A	1.20	**0.50**	1.48	0.73
2000 A	4.65	**2.14**	4.93	2.32
4000 A	3.81	**1.97**	5.24	2.18

Table 9. Comparison of THD of PCC bus currents for scenario no. 2.

	THD (I_{PCCbus}) (%)			
	With bus voltage control		Without bus voltage control	
Load type	Without active filtering	With active filtering	Without active filtering	With active filtering
100 A	1.12	**0.42**	1.36	0.61
2000 A	5.18	**2.53**	5.32	2.89
4000 A	4.83	**2.34**	5.18	2.62

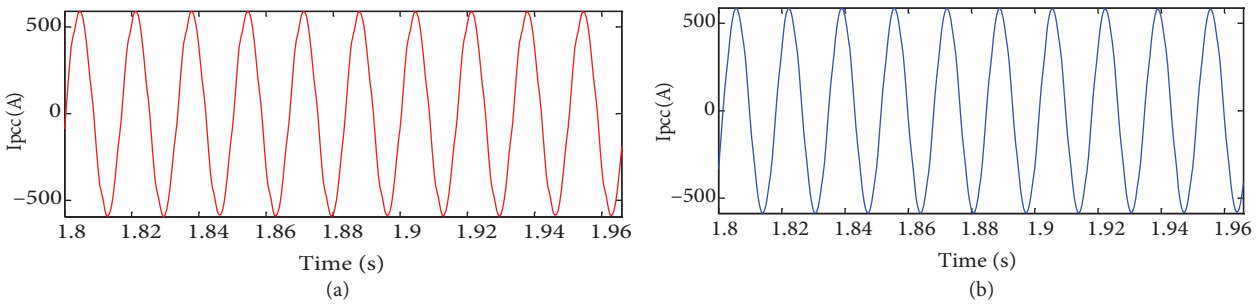

Figure 16. PCC bus current for load type 4000 A in scenario no. 2; (a) without control, (b) with proposed control method

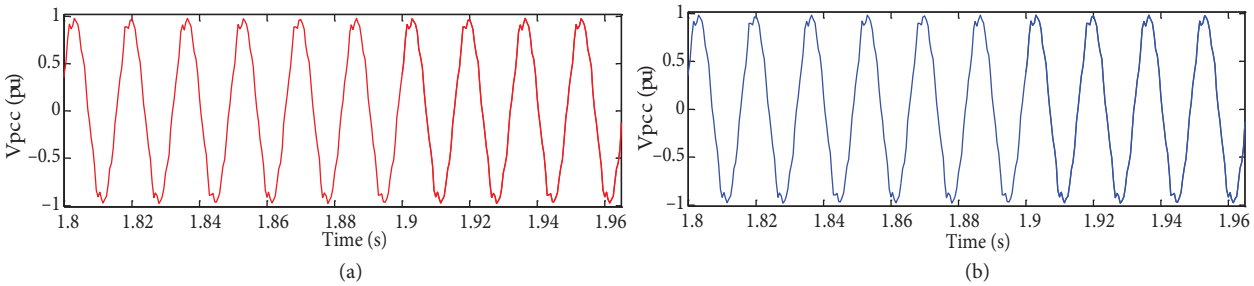

Figure 17. PCC bus voltage for load type 4000 A in scenario no. 2; (a) without control, (b) with proposed control method.

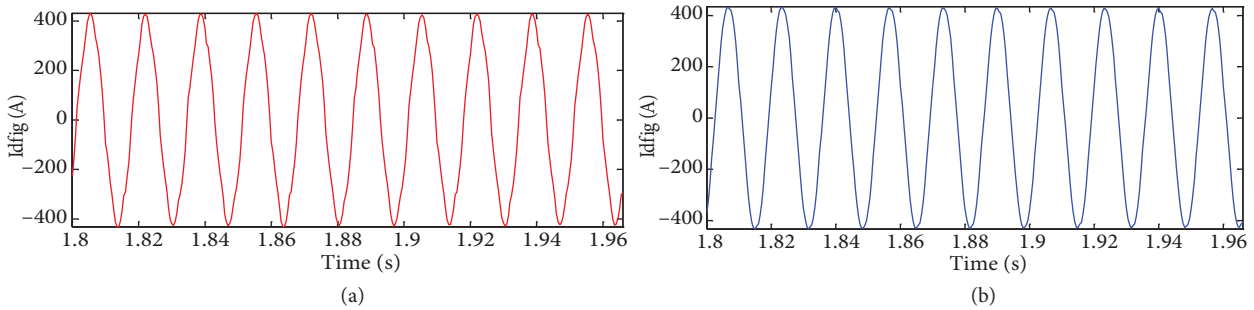

Figure 18. DFIG bus current for load type 4000 A in scenario no. 2; (a) without control, (b) with proposed control method.

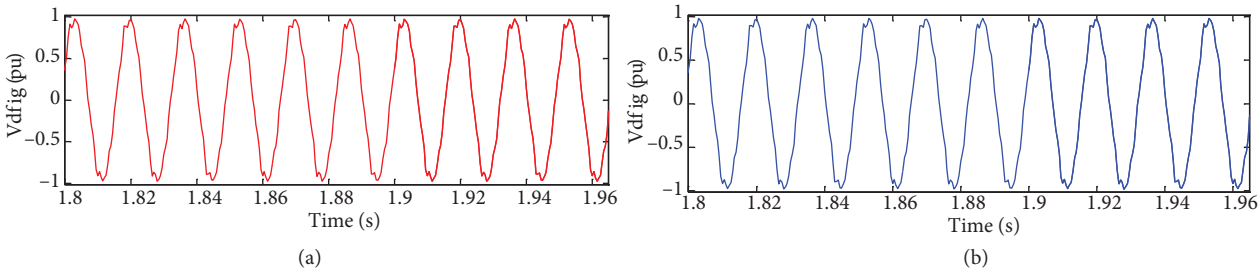

Figure 19. DFIG bus voltage for load type 4000 A in scenario no. 2; (a) without control, (b) with proposed control method.

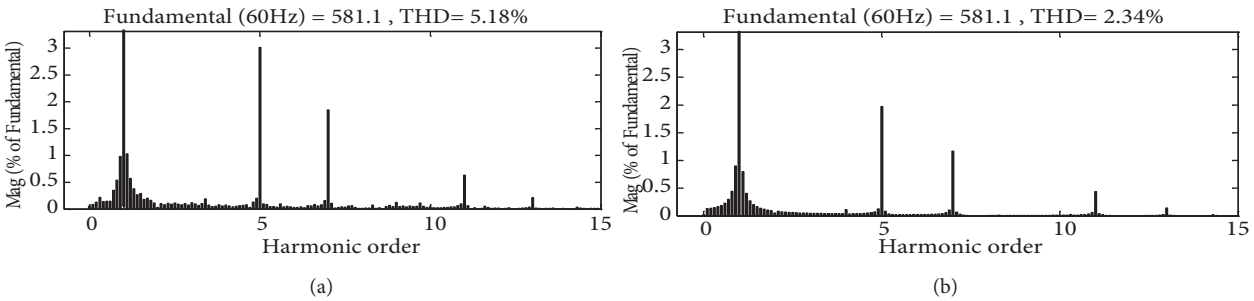

Figure 20. PCC bus current harmonic spectrum for load type 4000 A in scenario no. 2; (a) without control, (b) with proposed control method.

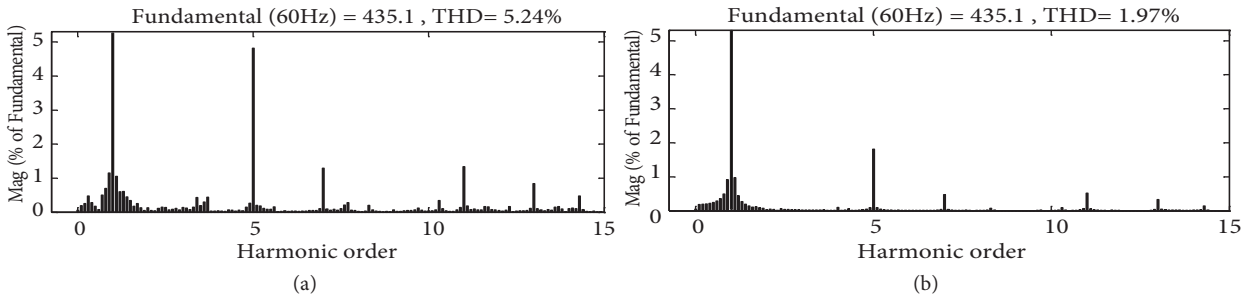

Figure 21. DFIG bus current harmonic spectrum for load type 4000 A in scenario no. 2; (a) without control, (b) with proposed control method.

6.3. Scenario no. 3: step change in NLL for local control condition

In this scenario a load variation is applied from 1700 A to 3500 A at t = 2 s with the wind speed constant and equal to 10 m/s for local control condition (NLL at bus 8).

As an example, the performances of the proposed active filtering capability of the DFIG for the compensation of harmonic currents with a step change of the NLL are shown in Figure 22 for the PCC bus. After the NLL step, the THD of the PCC bus current with and without the proposed control method is equal to 7.44% and 11.31%, respectively. The THD of the DFIG bus is equal to 6.14% with the control method and equal to 15.81% without it after the load step change. These are shown in Figure 23. These numbers show the effectiveness of the proposed method for this condition.

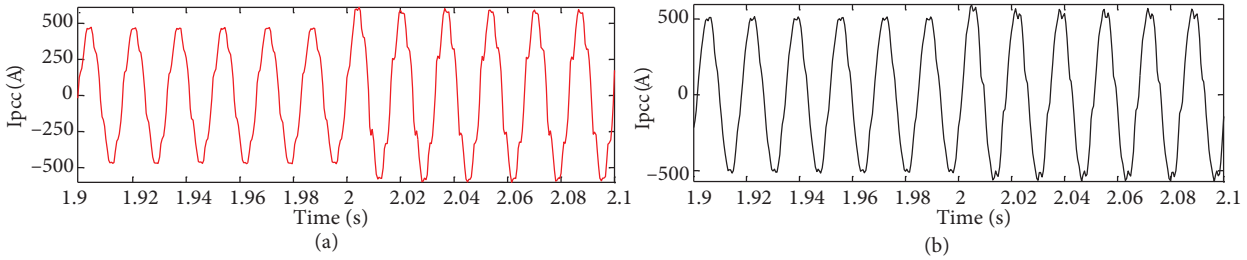

Figure 22. PCC bus current for step load change in scenario no. 3; (a) without control, (b) with proposed control method.

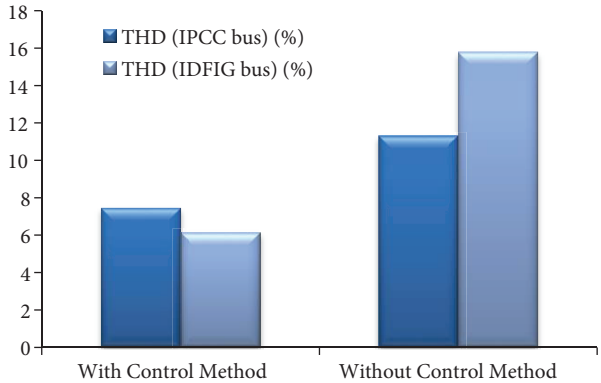

Figure 23. Currents THD after a step change in NLL with and without the proposed control method in local control condition (scenario no. 3).

6.4. Scenario no. 4: step change in NLL for remote control condition

In this scenario a load variation is applied from 1500 A to 2500 A at t = 2 s with the wind speed constant and equal to 10 m/s for remote control condition (NLL at bus 6). The performances of the proposed active filtering capability of the DFIG for the compensation of harmonic currents after a step of the NLL are shown in Figure 24. As illustrated in this figure, after the NLL step, the THD of the PCC bus current with and without the proposed control method is equal to 3.15% and 5.60%, respectively. Moreover, the THD of the DFIG bus is equal to 2.97% with the control method and equal to 6.58% without it after the load step change. These numbers in this figure show the suitable performance of the proposed method for this condition too.

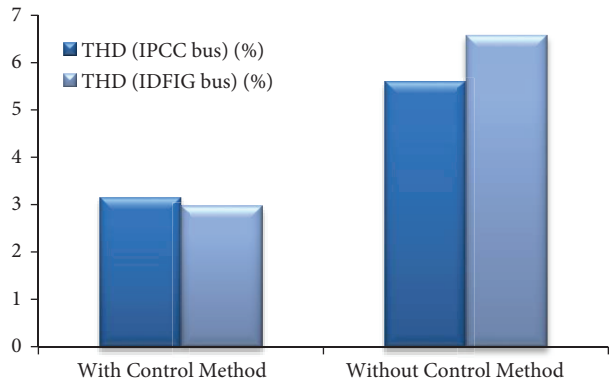

Figure 24. Currents THD after a step change in NLL with and without the proposed control method in remote control condition (scenario no. 4).

7. Conclusion

In this paper, in order to mitigate power system harmonics, a filtering technique is applied to a DFIG wind turbine control mechanism. A high selectivity filter is also used to determine grid side converter reference current. In addition, a new control strategy is used for bus voltage control. Using these two methods together in the power system, THD percent and harmonics will be decreased. To verify the performance of the proposed method, four operational scenarios for a nonlinear load (local and remote conditions for nonlinear load related to DFIG location and nonlinear load changes in these situations) are considered. Therefore, the assessment of the proposed method effectiveness is performed in normal and contingency conditions for both local and remote control situations. The proposed method is applied to a modified power system and the mentioned scenarios are considered too. As can be seen, the proposed methodology can manage the harmonic reduction issue in each scenario such as local and remote control. Furthermore, the presented strategy can reduce the system harmonics in the load change condition as a contingency condition for both local and remote situations. Therefore, the results of this technique show the excellent performance of this approach.

References

[1] Lobos T, Rezmer J, Sikorski T, Waclawek Z. Power distortion issues in wind turbine power systems under transient states. Turk J Elec Eng & Comp Sci 2008; 16: 229-238.

[2] Bharanikumar R, Kumar A.N. Performance analysis of wind turbine-driven permanent magnet generator with matrix converter. Turk J Elec Eng & Comp Sci 2012; 20: 299-317.

[3] Eggert B. 1.5 MW wind power station with low ac-line distortion using a standard doubly-fed generator system with field orientation control. In: 7th European Conference on Power Electronic and Applications; 1997; pp. 739-742.

[4] Kesraoui M, Chaib A, Meziane A, Boulezaz A. Using a DFIG based wind turbine for grid current harmonics filtering. Energy Conv Management 2014; 78: 968–975.

[5] Tentzerakis ST, Papathanassiou SA. An investigation of the harmonic emissions of wind turbines. IEEE T Energy Conv 2007; 22: 150-158.

[6] Lindholm M, Rasmussen TW. Harmonic analysis of doubly fed induction generators. In: Fifth International Conference on Power Electronic and Drive Systems; 2003; pp. 837-841.

[7] Fan L, Yuvarajan S, Kavasseri R. Harmonic analysis of a DFIG for a wind energy conversion system. IEEE T Energy Conv 2010; 25: 181-190.

[8] Liao Y, Ran L, Putrus GA, Smith KS. Evaluation of the effects of rotor harmonics in a doubly-fed induction generator with harmonic induced speed ripple. IEEE T Energy Conv 2003; 18: 508-515.

[9] Todeschini G, Emanuel AE. A novel control system for harmonic compensation by using wind energy conversion based on DFIG technology. In: Twenty-Fifth Annual IEEE Applied Power Electronics Conference and Exposition; 21–25 February 2010; pp. 2096-2103.

[10] BehzadJazi B, Abyaneh HA, Abedi M. Power quality improvement using active filter capability in back to back convertor installed for variable speed DFIG wind energy system. In: 19th Iranian Conference on Electrical Engineering (ICEE); 2011.

[11] Hoseinpour A, Barakati SM, Ghazi R. Harmonic reduction in wind turbine generators using a shunt active filter based on the proposed modulation technique. Elec Power Energy Sys 2012; 43: 1401–1412.

[12] Fan L, Yin H, Miao Z. A novel control scheme for DFIG-based wind energy systems under unbalanced grid conditions. Elec Power Sys Research 2011; 81: 254-262.

[13] Mohseni M, Masoum MAS, Islam SM. Low and high voltage ride-through of DFIG wind turbines using hybrid current controlled converters. Elec Power Sys Research 2011; 81: 1456-1465.

[14] Farhoodnea M, Mohamed A, Shareef H, Zayandehroodi H. Power quality impacts of high-penetration electric vehicle stations and renewable energy-based generators on power distribution systems. Measurement 2013; 46: 2423-2434.

[15] Shahbazi M, Poure P, Saadate S, Zolghadri MR. Five-leg converter topology for wind energy conversion system with doubly fed induction generator. Renewable Energy 2011; 36: 3187-3194.

[16] Comesana PF, Freijedo FD, Gandoy JD, Lopez O, Yepes AG, Malvar J. Mitigation of voltage sags, imbalances and harmonics in sensitive industrial loads by means of a series power line conditioner. Elec Power Sys Research 2012; 84: 20-30.

[17] Fan L, Kavasseri R, Yin H, Zhu C, Hu M. Control of DFIG for rotor current harmonics elimination. In: IEEE 2009 Power & Energy Society General Meeting; 2009.

[18] Jain AK, Ranganathan VT. Wound rotor induction generator with sensorless control and integrated active filter for feeding nonlinear loads in a stand-alone grid. IEEE T Indus Elect 2008; 55: 218-228.

[19] Gaillard A, Poure P, Saadate S, Machmoum M. Variable speed DFIG wind energy system for power generation and harmonic current mitigation. Renewable Energy 2009; 34: 1545-1553.

[20] Chowdhury BH, Chellapilla S. Double-fed induction generator control for variable speed wind power generation. Elec Power Sys Research 2006; 76: 786-800.

[21] Poitiers F, Bouaouiche T, Machmoum M. Advanced control of a doubly-fed induction generator for wind energy conversion. Elec Power Sys Research 2009; 79: 1085-1096.

[22] Karimi-Davijani H, Sheikholeslami A, Livani H, Norouzi N. Fault ride-through capability improvement of wind farms using doubly fed induction generator. In: UPEC 43rd International Conference Universities Power Engineering; 2008.

[23] Akagi H, Watanabe EH, Aredes M. Instantaneous Power Theory and Applications to Power Conditioning. Piscataway, New Jersey, USA: IEEE Press—Wiley InterScience, 2007.

[24] Vas P. Sensorless Vector and Direct Torque Control. Oxford, UK: Oxford University Press, 1998.

[25] Katiraei F, Iravani MR, Lehn PW. Micro-grid autonomous operation during and subsequent to islanding process. IEEE T Power Del 2005; 20: 248-257.

Appendix

<table>
<tr><td>Generator Parameters:</td><td>DC-link Parameters:</td></tr>
<tr><td>P_{nom}=4.5 MW, cosφ=0.9, V$_{nom}$=575 v, p=3</td><td>$V_{dc-link}$=1200 v, C$_{dc-link}$=0.03 F</td></tr>
<tr><td>R_s=0.007060 pu, L$_{ls}$=0.171 pu, R$_r$=0.005 pu</td><td>Grid Side Parameters:</td></tr>
<tr><td>L_{lr}=0.151 pu, L$_m$=2.9 pu, H=5.04 s, F=0.01 pu</td><td>Rg=0.003 pu, L$_g$=0.3 pu</td></tr>
<tr><td>HSF Parameters:</td><td>NLL Parameters:</td></tr>
<tr><td>K=80, ω=2*π*60</td><td><table><tr><td>Load Type</td><td>R (Ω)</td><td>L (mH)</td></tr><tr><td>100 A</td><td>7.7</td><td>9.1</td></tr><tr><td>2000 A</td><td>0.37</td><td>1</td></tr><tr><td>4000 A</td><td>0.18</td><td>0.5</td></tr></table></td></tr>
</table>